BIOCHEMISTRY
including biophysical chemistry & molecular biology
Article

Biochemistry **2010,** *49,* 4361–4373 4361
DOI: 10.1021/bi100092a

Probing DNA Binding, DNA Opening, and Assembly of a Downstream Clamp/Jaw in *Escherichia coli* RNA Polymerase−λP_R Promoter Complexes Using Salt and the Physiological Anion Glutamate†

Wayne S. Kontur,[‡,∥,⊥] Michael W. Capp,[§,∥] Theodore J. Gries,[§,∥] Ruth M. Saecker,*[,§] and M. Thomas Record, Jr.*[,‡,§]

[‡]*Department of Chemistry, and* [§]*Department of Biochemistry, University of Wisconsin, Madison, Wisconsin 53706* [∥]*These authors contributed equally to this work.* [⊥]*Current address: Department of Bacteriology, University of Wisconsin/Great Lakes Bioenergy Research Center, Madison, WI 53706.*

Received January 20, 2010; Revised Manuscript Received February 26, 2010

ABSTRACT: Transcription by all RNA polymerases (RNAPs) requires a series of large-scale conformational changes to form the transcriptionally competent open complex RP_o. At the λP_R promoter, *Escherichia coli* σ^{70} RNAP first forms a wrapped, closed 100 bp complex I_1. The subsequent step opens the entire DNA bubble, creating the relatively unstable (open) complex I_2. Additional conformational changes convert I_2 to the stable RP_o. Here we probe these events by dissecting the effects of Na^+ salts of Glu^-, F^-, and Cl^- on each step in this critical process. Rapid mixing and nitrocellulose filter binding reveal that the binding constant for I_1 at 25 °C is ∼30-fold larger in Glu^- than in Cl^- at the same Na^+ concentration, with the same log−log salt concentration dependence for both anions. In contrast, both the rate constant and equilibrium constant for DNA opening (I_1 to I_2) are only weakly dependent on salt concentration, and the opening rate constant is insensitive to replacement of Cl^- with Glu^-. These very small effects of salt concentration on a process (DNA opening) that is strongly dependent on salt concentration in solution may indicate that the backbones of both DNA strands interact with polymerase throughout the process and/or that compensation is present between ion uptake and release. Replacement of Cl^- with Glu^- or F^- at 25 °C greatly increases the lifetime of RP_o and greatly reduces its salt concentration dependence. By analogy to Hofmeister salt effects on protein folding, we propose that the excluded anions Glu^- and F^- drive the folding and assembly of the RNAP clamp/jaw domains in the conversion of I_2 to RP_o, while Cl^- does not. Because the Hofmeister effect of Glu^- or F^- largely compensates for the destabilizing Coulombic effect of any salt on the binding of this assembly to downstream promoter DNA, RP_o remains long-lived even at 0.5 M Na^+ in Glu^- or F^- salts. The observation that $E\sigma^{70}$ RP_o complexes are exceedingly long-lived at moderate to high Glu^- concentrations argues that $E\sigma^{70}$ RNAP does not dissociate from strong promoters in vivo when the cytoplasmic glutamate concentration increases during osmotic stress.

Escherichia coli cells have the remarkable ability to grow over a very wide range of environmental conditions, including osmotic conditions ranging from very dilute (0.02 osmolal) to concentrated, high-salt media (> 3 osmolal) (*1*−*3*). In vivo, increases in external osmolarity, which increase cytoplasmic K^+ and Glu^- concentrations, reduce the level of bulk transcription (*4*), while the level of transcription from genes involved in the osmotic stress response selectively increases (*5*−*7*). In the absence of any known osmosensing (e.g., glutamate binding) transcription factor, the simplest hypothesis is that changes in cytoplasmic K^+ and Glu^- concentrations alone alter transcription (*8*) during the initial response to an osmotic upshift. What features of RNA polymerase and promoter sequence allow the cell to achieve a dramatic reprogramming to maintain homeostasis?

Understanding how cells regulate their gene expression requires kinetic−mechanistic studies. Although transcription by *E. coli* RNAP[1] has been studied in vivo and in vitro for four decades, we are only beginning to understand the workings of this machine at a molecular level. How is DNA opened by RNAP, and what significant conformational changes occur during the steps that precede and follow this central DNA opening step? How do variables like the identity of the σ specificity subunit, the promoter DNA sequence, supercoiling, concentrations of solutes, small ligands, or regulatory proteins affect the rate of formation and lifetime of the transcriptionally competent open complex and thereby alter the frequency of productive versus abortive initiation from the promoter?

Because the RNAP machinery and promoter organization are conserved, it is likely that the sequence of conformational changes that form the bacterial RP_o is largely invariant (promoter DNA recognition, DNA opening, and stabilization of RP_o) but that the rates of interconversion and populations of

†This work was supported by National Institutes of Health (NIH) grants GM23467 and GM47022 to M.T.R. W.S.K. gratefully acknowledges the support of the Biotechnology Training Program (NIH Grant 5 T32 GM08349). T.J.G. is the recipient of the William R. and Dorothy E. Sullivan Distinguished Graduate Fellowship.

*To whom correspondence should be addressed. Telephone: (608) 262-5332. Fax: (608) 262-3453. E-mail: mtrecord@wisc.edu or rmsaecker@wisc.edu.

[1]Abbreviations: ASA, water-accessible surface area; GB, glycine betaine; PNAI, protein nucleic acid interactions; RNAP, RNA polymerase; σ^S, stationary phase σ factor.

Published on Web 03/04/2010

initiation intermediates differ as a function of the variables noted above. Here we investigate how the substitution of the physiological anion Glu^- for the laboratory anion Cl^- affects each step in the process of open complex formation at the λP_R promoter by the housekeeping form of *E. coli* RNA polymerase (RNAP, subunit composition $\sigma^{70}\alpha_2\beta\beta'\omega$). While our research focuses on this promoter, we expect that these results reflect the salient functional characteristics of many Eσ^{70} RNAP−promoter interactions.

In vitro, changes in salt concentration profoundly affect both the composite second-order association rate constant (k_a) and the composite dissociation rate constant (k_d) for the formation and dissociation of RP_o at the λP_R promoter, respectively (*9*, *10*). One contributor to these salt effects is Coulombic: positively charged residues in the promoter−RNAP interface reduce the high negative phosphate charge density of DNA, releasing locally accumulated salt ions (e.g., K^+ or Na^+ from DNA). In addition, the identity of the anion has large effects on the magnitude of k_a: for the λP_R promoter, k_a was found to be at least 30-fold larger in glutamate (Glu^-) than in chloride (Cl^-) at 0.20 M K^+ (*11*). Here we dissect this large salt anion effect. Large effects of substitution of another anion for Cl^- are also observed for many other nucleic acid binding proteins, including transcription factors (*12*−*14*), helicases (*13*), T7 RNAP (*15*), and DNA polymerases. Large Hofmeister effects of salt anions like Glu^- and F^-, relative to Cl^-, are expected on steps in which interface formation or coupled folding buries large amounts of nonpolar (hydrocarbon) surface (*16*, *17*, D. Belissimo et al., unpublished observations).

At the strong λP_R promoter (P), the mechanism of formation of the open complex consists of a minimum of three steps, proceeding through two kinetically significant intermediates (*9*, *18*−*20*)

$$R + P \underset{k_{-1}}{\overset{k_1}{\rightleftarrows}} I_1 \underset{k_{-2}}{\overset{k_2}{\rightleftarrows}} I_2 \underset{k_{-3}}{\overset{k_3}{\rightleftarrows}} RP_o \qquad \text{(mechanism I)}$$

where R represents Eσ^{70} RNAP, P is the promoter, and I_1 and I_2 are the first and second kinetically significant intermediates, respectively. Opening of the entire DNA bubble (positions −11 to +2) occurs in the conversion of I_1 to I_2 (*21*, *22*). No other early intermediates are kinetically significant at the λP_R promoter. Solute upshift studies designed to study the late steps in RP_o formation reveal the existence of an intermediate (I_3) formed after I_2 and directly preceding the formation of RP_o (*23*). I_3 rapidly equilibrates with I_2 and RP_o under the conditions of this study and thus can be neglected in the analysis of k_d presented here. Because the kinetics of open complex formation (association) and dissociation are single-exponential for almost all conditions examined, we deduce that (i) in association, I_1 rapidly equilibrates with free RNAP and promoter DNA on the time scale required for I_1 to convert to I_2 ($k_{-1} \gg k_2$) and (ii) I_2 rapidly equilibrates with RP_o on the time scale required for I_2 to convert to I_1 in the reverse direction ($k_3 \gg k_{-2}$). The interconversions of I_1 and I_2 are the bottleneck steps in both the association and dissociation directions.

Using rapid mixing, we recently dissected the composite association and dissociation rate constants for RNAP−λP_R interactions into their individual contributions from K_1 ($=k_1/k_{-1}$), k_2, k_{-2}, and K_3 ($=k_3/k_{-3}$) (*20*, *23*). We discovered that destabilizing RP_o by a rapid upshift in salt or urea concentration creates a transient burst of I_2 (*23*). Coupling rapid mixing with filter binding, we determined the kinetics of forming this unstable open complex (I_2) from the stable open complex RP_o and converting I_2 to the closed complex I_1 over a wide range of salt concentrations at 10 and 37 °C. These studies dissected the effect of salt concentration on the dissociation kinetics for the first time. The rate constant k_{-2} is independent of salt concentration, while the equilibrium constant for the conversion of I_2 to RP_o decreases strongly with an increase in salt concentration (*23*). Permanganate footprinting of I_2 reveals that all reactive thymines in RP_o are also reactive in I_2, demonstrating that the entire transcription bubble is opened in the rate-determining step $I_1 \rightarrow I_2$ (*22*). Measurements of the time dependence of the decay of permanganate reactivity in the conversion of I_2 to I_1 corroborate the value of k_{-2} obtained by rapid mixing and filter binding.

The unexpected result that the rate constant k_{-2} characterizing the conversion of I_2 to the transition state $(I_1-I_2)^{\ddagger}$ is independent of salt concentration motivates the work here to dissect the effects of salt concentration on the steps of the first half of the mechanism, namely, the formation of I_1 and the transition between I_1 and $(I_1-I_2)^{\ddagger}$. Melting of DNA in solution is strongly dependent on salt concentration (*24*). How does melting DNA to form the initiation bubble in the isomerization of I_1 to I_2 compare?

To address this question, we examine whether rate constant k_2 characterizing the conversion of I_1 to $(I_1-I_2)^{\ddagger}$ is dependent on salt concentration. Using rapid mixing and filter binding, we dissect for the first time the overall second-order association rate constant k_a into K_1 and k_2 over a range of NaCl and NaGlu concentrations. In addition, we obtain stringent tests of the single-exponential character of both the association kinetic data (in excess RNAP) and dissociation kinetic data. These findings demonstrate that the initial steps of association (forming I_1) and dissociation (forming I_2) do indeed rapidly equilibrate on the time scale of the subsequent slower conformational change (DNA opening or closing). We use manual mixing filter binding to examine the effects of salt concentration (NaX) and choice of anion (X = Cl^-, Glu^-, or F^-) on the dissociation of RP_o at 25 °C.

We find that each step exhibits a uniquely different dependence on changes in Na^+ concentration and choice of anion. While the formation of I_1 and conversion of I_2 to RP_o exhibit large dependences on both Na^+ concentration and anion, the bottleneck DNA opening step ($I_1 \rightarrow I_2$) is relatively insensitive to either solution variable. Formation of I_1 and especially formation of RP_o are greatly favored in Glu^- relative to Cl^-. Together, these results shed additional light on the conformational changes occurring in each step, allowing us to refine our current structural−mechanistic hypotheses regarding formation of the open complex by *E. coli* RNAP. In particular, we propose that the very large effects of replacing Cl^- with Glu^- on the steps after DNA opening result from burial of hydrocarbon surface of RNAP in coupled folding transitions in late steps (*23*, *25*, *26*). Glu^- and F^- are more highly excluded from nonpolar surface than Cl^- is (*16*, *17*, D. Belissimo et al., unpublished observations). We deduce that these late remodeling events assemble a RNAP clamp/jaw on downstream DNA and contribute significantly to the entropic driving force that stabilizes the open DNA state in RP_o.

MATERIALS AND METHODS

Buffers. Storage buffer (SB) for the RNA polymerase holoenzyme contained 50% glycerol (v/v), 10 mM Tris-HCl (pH 7.5 at 4 °C), 100 mM NaCl, 0.1 mM dithiothreitol (DTT), and 0.1 mM

Na_2EDTA. Binding buffer for the study of the kinetics of RNAP−promoter binding as a function of univalent salt concentration in the absence of Mg^{2+} (BB) contained 10 mM Na_2HPO_4 buffer (pH 7.4), 6.5% (v/v) glycerol, 1 mM DTT, 100 μg/mL BSA, 1.3 mM Tris (pH 7.5 at 4 °C; contributed by storage buffer), and variable NaCl, NaGlu, or NaF concentrations to bring the Na^+ concentration to the desired value. Wash buffer (WB) contained 0.1 M NaCl, 10 mM Tris-HCl (pH 8.0 at room temperature), and 0.1 mM Na_2EDTA. Addition of NaGlu did not significantly affect the pH of the Tris-HCl buffer.

Wild-Type Eσ^{70} RNA Polymerase Holoenzyme. *E. coli* K12 wild-type RNA polymerase holoenzyme was purified as described in ref *27* except that the final Bio-Rex 70 chromatography step was replaced with a phosphocellulose column and run in 50% glycerol-containing buffer (*28*). Purified RNAP was stored in SB at −70 °C. All RNAP concentrations reported here are concentrations of the active holoenzyme (capable of RP_o formation). Activities were determined at the time of use, either by analysis of forward titrations of promoter DNA with RNAP performed in the "complete binding of limiting reagent" regime at 37 °C as described previously (*9*) or by comparison of association rate constants for different samples determined at the same total RNAP concentration. Typically, activities were ∼70%. Systematic comparisons of the different preparations showed no difference in promoter association kinetics between individual tubes or preps, when compared at the same active RNAP concentration.

λP$_R$ Promoter DNA. A [^{32}P]DNA fragment containing the λP_R promoter was obtained from plasmid pBR81 as described in ref *29*. BssHII and SmaI cleavage of pBR81 centrally positions the λP_R wild-type sequence (−60 to +20) in a fragment that extends from −115 to +76 relative to the transcription start site (+1) of the promoter. The specific activity of the fragment was generally ∼10^9 cpm/mol.

Association Kinetics. For conditions under which the kinetics are sufficiently slow [e.g., RNAP concentrations of < 10 nM at midrange salt concentrations; high (> 0.3 M) salt concentrations], manual mixing and filter binding were used to determine the kinetics of formation of long-lived (open) complexes, resistant to a 10−30 s heparin challenge. For conditions under which the kinetics are too fast (first-order rate constant k_{obs} > 0.01 s^{-1}) to determine by manual mixing (e.g., low salt and higher RNAP concentrations), rapid mixing (2 ms mixing time; RQF-3, Kintek Corp., Austin, TX) followed by filter binding of quenched solutions was used (*20*). Rapid mixing and manual mixing experiments were performed as described in ref *20*. Concentrations of active RNAP were always in large excess over that of promoter to ensure that the initial bimolecular binding step is pseudo-first-order within experimental uncertainty.

Dissociation Kinetics. (*i*) *Irreversible Dissociation Initiated via Addition of Heparin to Preformed RP$_o$*. Effects of Na^+ concentration in Cl^- buffer on the dissociation of preformed λP_R DNA (0.08−0.09 nM) and RNAP (10 − 40 nM) open complexes at 25 °C were assessed as described in ref *26*.

(*ii*) *Decay-to-Equilibrium Assay To Determine k$_d$*. The irreversible dissociation of RP_o complexes initiated by the addition of excess heparin is exceedingly slow in Glu^- at 25 °C, yielding poorly determined values of k_d. Thus, to determine k_d as a function of Na^+ in Glu^- buffer, we used a decay-to-equilibrium assay at a low RNAP concentration held constant by an excess of the competitor heparin. In this assay, 7 nM RNAP was initially mixed with a vast excess of heparin (0.1−1 mg/mL) at the salt concentration used in the experiment. After incubation for 60 min, ^{32}P-labeled λP_R DNA (12.5 pM) was added, initiating promoter binding which proceeds to equilibrium at the low RNAP concentration used in the experiment. The amount of λP_R−RNAP open complexes was monitored using nitrocellulose filter binding. Typically, > 10^5 s was required to approach promoter binding equilibrium. At longer times, a very slow decay of the plateau was noted, probably the result of inactivation of RNAP.

Nitrocellulose Filter Binding Assays. The amount of promoter DNA in open complexes as a function of time and solution conditions was determined using nitrocellulose filter binding as described in ref *20*. Studies in Glu^- and F^- cannot be performed above 0.60 M Na^+ because filter efficiency becomes too low.

DATA ANALYSIS

Data were analyzed using either SigmaPlot 6.0 or 2000 (SPSS, Inc., Chicago, IL) on a Dell Optiplex GX270 workstation running Windows XP Professional version 2002 (Microsoft, Seattle, WA), or using Igor 5.0.3.0 (WaveMetrics, Inc., Lake Oswego, OR) on Dell Inspiron 8100 computer.

Determination of k$_{obs}$, k$_a$, K$_1$, and k$_2$ from the Kinetics of Formation of Open Complexes. In excess RNAP, the kinetics of irreversible association of RNAP with λP_R promoter DNA to form open complexes (I_2, RP_o) are single-exponential (see Results) with observed rate constant k_{obs}, determined by fitting the fraction of promoter DNA bound in open complexes at time t (θ_t^{open}) (calculated as described in ref *20*) versus time to eq 1:

$$\theta_t^{open} = 1 - e^{-k_{obs}t} \quad (1)$$

The rate constant k_{obs} (previously called α_{CR}) is a hyperbolic function of RNAP concentration (*20*):

$$k_{obs} = \frac{K_1 k_2 [RNAP]}{1 + K_1[RNAP]} = \frac{k_a[RNAP]}{1 + K_1[RNAP]} \quad (2)$$

where K_1 ($= k_1/k_{-1}$) is the equilibrium constant for formation of I_1, k_2 is the microscopic rate constant for the subsequent (rate-determining) conversion of I_1 to I_2 in mechanism I, and k_a ($= K_1k_2$) is the composite overall second-order association rate constant. The data for k_{obs} as a function of RNAP concentration in Figures 3 and 4 were weighted by $1/\sigma^2$, where σ is the standard deviation of k_{obs}, and fit to eq 2 to determine values of k_a, K_1, and k_2 at each salt concentration investigated.

Above 0.23 M Na^+ in NaCl buffer and 0.29 M Na^+ in NaGlu buffer, k_{obs} increases linearly with RNAP concentration up to the highest accessible concentration (∼120 nM), indicating (eq 2) that K_1[RNAP] ≪ 1. In this limit, the overall association rate constant k_a was determined using the following equation:

$$k_a = (k_{obs}/[RNAP])(1 + K_1[RNAP]) \approx k_{obs}/[RNAP] \quad (3)$$

The quality of the approximation was estimated by linear extrapolation of the log−log plots of K_1 versus RNAP concentration (Figure 4A) and found to be appropriate.

Determination of the Composite Dissociation Rate Constant k$_d$. (i) The observed rate constant k_d for the irreversible dissociation of open complexes was determined by fitting θ_t^{open} versus time at a given Na^+ concentration to a single-exponential

decay equation

$$\theta_t^{\text{open}} = \theta_{t=0}^{\text{open}} e^{-k_d t} \quad (4)$$

where $\theta_{t=0}^{\text{open}}$ is the value of θ_t^{open} at time zero.

(ii) The promoter dissociation rate constant (k_d) and the RNAP−heparin binding constant (K_{heparin}) at 25 °C in Glu^- and F^- buffers were determined from the observed decay-to-equilibrium (relaxation) rate constant k_r (see below) and the RNAP−promoter association rate constant k_a (see below). The data were modeled using the following mechanism:

$$\begin{array}{ll} R + H \overset{K_{\text{heparin}}}{\rightleftarrows} HR & \text{rapid equilibrium} \\ R + P \underset{k_d}{\overset{k_a}{\rightleftarrows}} RP_o & \text{slow to equilibrate} \end{array} \quad \text{(mechanism II)}$$

In mechanism II, H is heparin, P is promoter DNA, R is free RNAP, and RP_o is the final open complex (concentrations of intermediates are negligible). K_{heparin} is the equilibrium constant for the formation of a heparin−RNAP complex; this equilibrates rapidly on the time scale of association of RNAP with promoter DNA. The composite rate constants for formation (k_a) and dissociation (k_d) of RP_o are defined by eqs 2 and 4, respectively. Our analysis of mechanism II assumes one heparin binding site on RNAP and applies to conditions where $[H]_{\text{total}} \gg [R]_{\text{total}} \gg [P]_{\text{total}}$. For this situation, the experimentally determined approach-to-equilibrium rate constant $k_r = d[\ln(\theta_{t=\infty}^{\text{open}} - \theta_t^{\text{open}})]/dt = k_a[R] + k_d$, where [R] is the free RNAP concentration. [R] is constant in these assays (though not in excess over promoter) because the heparin binding equilibrium buffers its free concentration. The integrated form of this equation is used to determine k_d:

$$\theta_t^{\text{open}} = \frac{k_a[R][1 - e^{-(k_a[R]+k_d)t}]}{k_a[R] + k_d} \quad (5)$$

where [R] is determined from eq 6:

$$[R] = \frac{[R]_{\text{total}}}{1 + K_{\text{heparin}}[H]_{\text{total}}} \quad (6)$$

For the set of relaxation data collected as a function of $[H]_{\text{total}}$ at a given Na^+ concentration in Glu^- or F^- buffer, data at each heparin concentration were fit to eqs 5 and 6, using the value of k_a determined from the independent kinetics of association experiments (Table 1). Reported values of K_{heparin} and k_d for each salt condition represent the average and standard deviation from these individual fits.

RESULTS

Single-Exponential Kinetics of Formation of E. coli RNA Polymerase−λP$_R$ Promoter Complexes: Effects of Glutamate and Chloride Salts. To compare the effects of the laboratory anion chloride (Cl^-) and the physiological anion glutamate (Glu^-) on the binding of *E. coli* RNAP to the λP_R promoter to form a closed complex and on the subsequent DNA opening step, we determined the kinetics of association over wide ranges of RNAP concentration (1−100 nM) and of chloride and glutamate concentrations (0.13−0.27 M Na^+ in Cl^- buffer and 0.23−0.64 M Na^+ in Glu^- buffer) at 25 °C. A limited number of association experiments were performed in F^- buffer at low RNAP concentrations to compare to the results in Glu^- buffer. Sodium salts were used because complexation of potassium by heparin interferes with the heparin challenge (see Materials and Methods) at high concentrations of potassium salts (*10*); Mg^{2+} was omitted because it forms a complex with glutamate (*30*). In most cases, the full accessible ranges of RNAP and of salt concentration were investigated.

Following either manual or rapid mixing, nitrocellulose filter binding was used to determine the kinetics of formation of long-lived, competitor-resistant complexes (RP_o). Representative kinetic data for selected low and high RNAP concentrations over the range of NaCl and NaGlu concentrations are plotted as the fraction of promoter DNA in open complexes (θ_t^{open}) as a function of time in Figures 1 and 2, respectively. The plateau at $\theta_t^{\text{open}} = 1$ observed at long times for all salt concentrations investigated demonstrates that open complex formation is irreversible and therefore directly interpretable in terms of the forward rate constant k_{obs} (see eq 1 in Data Analysis), without the need for a decay-to-equilibrium analysis. Irreversibility of the forward kinetics is confirmed by direct measurement of the dissociation rate constant (see below).

Single-exponential fits of these data to the irreversible first-order rate equation (eq 1) are shown in Figures 1 and 2. Values of k_{obs} determined from these fits are given in Tables 1 and 2 of the Supporting Information. To expand the initial (millisecond) time regime and examine whether the short time data provide any indication of a second (faster) decay, the insets to the panels of Figures 1 and 2 plot the same data as θ_t^{open} versus log t (cf. refs *53* and *54*). For the λP_R promoter and the conditions investigated previously (cf. refs *9*, *10*, *18*, and *20*) and in this study, all association kinetic data are well-described as single-exponential decays. Single-exponential kinetics of open complex formation indicate that the step forming the first kinetically significant intermediate (I_1) rapidly equilibrates with free promoter DNA on the time scale of the conversion of I_1 to I_2 (*19*).

The Observed Forward Rate Constant k_{obs} Is a Hyperbolic Function of RNAP Concentration over the Accessible Range. Values of the overall rate constant k_{obs} are plotted versus RNAP concentration in panels A (Cl^-) and B (Glu^-) of Figure 3 for the salt concentrations investigated. In most cases, these data cover a 100-fold range of RNAP concentrations (~1−100 nM). At all salt concentrations investigated, except the highest Glu^- concentration, values of k_{obs} exhibit the expected hyperbolic dependence on RNAP concentration (eq 2) with a well-defined plateau. There is no evidence of sigmoidicity in any of these plots at low RNAP concentrations, as would be predicted if dissociation of the holoenzyme into the σ subunit and core polymerase were significant at these concentrations of RNAP and salt (*31*). The observations of single-exponential association kinetics (Figures 1 and 2) and hyperbolic dependencies of k_{obs} on RNAP concentration (Figure 3) validate the use of eq 2 (Data Analysis) to analyze the dependence of k_{obs} on RNAP concentration and obtain k_2, the DNA opening rate constant, and K_1, the equilibrium constant for formation of I_1 (see Data Analysis).

DNA Opening by RNAP Is Relatively Slow and Only Weakly Dependent on Salt Concentration. Replacing Cl^- with Glu^- Has No Significant Effect on k_2 or on Its Log−Log Derivative Sk_2. Rate constants for the DNA opening step (k_2) are plotted on a log−log scale as a function of Na^+ concentration for experiments in Cl^- and Glu^- buffer in Figure 4A. Values of k_2 decrease very modestly with increasing salt concentration, from 0.35 s^{-1} at 0.15 M Na^+ in Cl^- buffer to 0.18 s^{-1} at 0.29 M Na^+ in Glu^- buffer, corresponding to time constants of 3−5 s for opening. Neither k_2 at 0.23 M salt (the overlap concentration in our experiments) nor Sk_2 is affected by

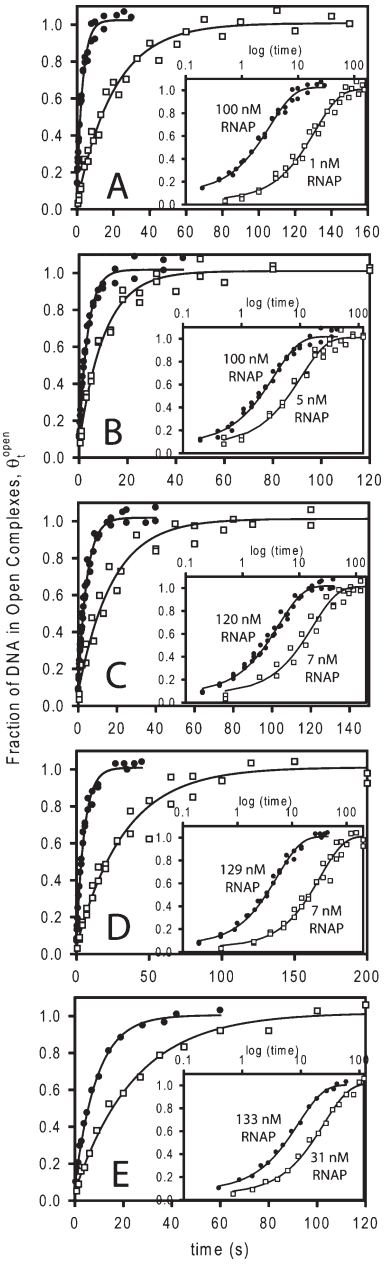

FIGURE 1: Representative kinetic data for formation of open complexes at the λP_R promoter at high (●) and low (□) concentrations of active RNAP (where RNAP is in excess over promoter DNA) at five different Na^+ concentrations at 25 °C in NaCl buffer. All data shown here were obtained using rapid quench mixing; the fraction of promoter DNA in the form of open complexes θ_t^{open} as a function of time (t) was determined using nitrocellulose filter binding after association reactions were quenched with the competitor heparin. Theoretical curves through the data are the best fits to eq 1; corresponding first-order irreversible rate constants (k_{obs}) for each RNAP concentration are given in Table 1 of the Supporting Information. Insets replot the data as a function of log t, demonstrating the single-exponential character of the kinetics over the entire time range: (A) 0.15, (B) 0.17, (C) 0.19, (D) 0.21, and (E) 0.23 M Na^+.

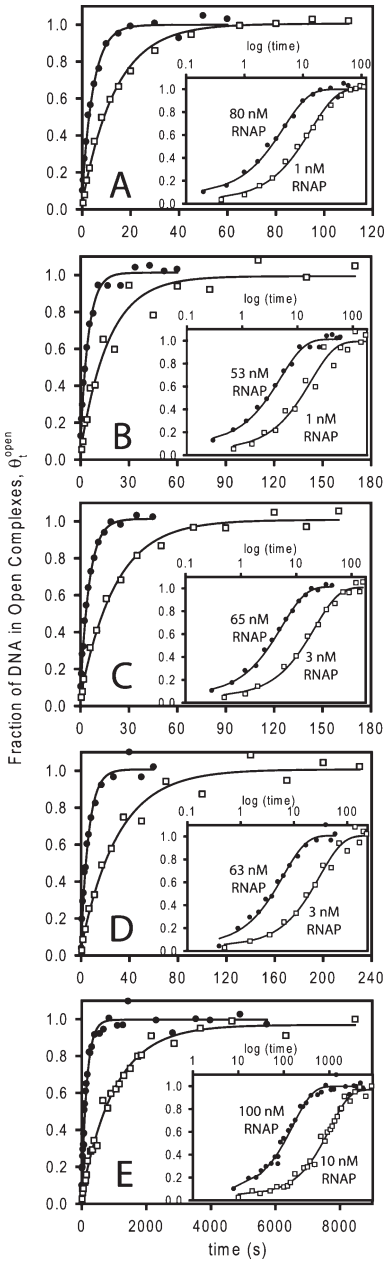

FIGURE 2: Representative kinetic data for formation of open complexes at the λP_R promoter at high (●) and low (□) concentrations of active RNAP at five different Na^+ concentrations at 25 °C in NaGlu buffer (details and insets as in Figure 1; values of k_{obs} for each RNAP concentration are given in Table 2 of the Supporting Information). With the exception of panel E, all data were obtained using rapid quench mixing: (A) 0.23, (B) 0.25, (C) 0.27, (D) 0.29, and (E) 0.55 M Na^+.

replacement of Cl^- with Glu^-; individual fits of these data yield Sk_2 values of -1.1 ± 0.1 and -0.9 ± 0.3 in Cl^- and Glu^- buffers, respectively. As shown in Figure 4A, the combined data fall on a common line with a log−log slope (Sk_2) of -1.1 ± 0.1. Previously, we found from KCl concentration upshift experiments at 10 and 37 °C in transcription buffer (10 mM $MgCl_2$) that the rate constant k_{-2} for the reverse direction of this step (I_2 to I_1) is independent of KCl concentration [$Sk_{-2} = 0$ (*23*)]. Interpolation between values yields a k_{-2} of ≈1.7 s^{-1} at 25 °C. Assuming this value of k_{-2} applies to the salt conditions investigated here, we obtain equilibrium constants (K_2) for DNA opening by RNAP (i.e., $I_1 \rightleftarrows I_2$) that decrease from 0.2 at 0.15 M salt to 0.1 at 0.29 M salt. I_2 is therefore unstable with respect to I_1 at all salt concentrations, and the salt concentration dependence of the DNA opening step is small ($SK_2 = Sk_2 - Sk_{-2} = -1.1 \pm 0.1$).

Formation of Wrapped I_1 Is Strongly Dependent on Salt Concentration ($SK_1 = -6.9 \pm 0.3$). Replacing Cl^- with Glu^- Increases K_1 ~30-fold without Significantly Affecting SK_1. The proposed RNAP−DNA interface in I_1 spans 100 bp; the net positive charge on RNAP in this interface is at least +37 (see Discussion). How dependent on salt concentration

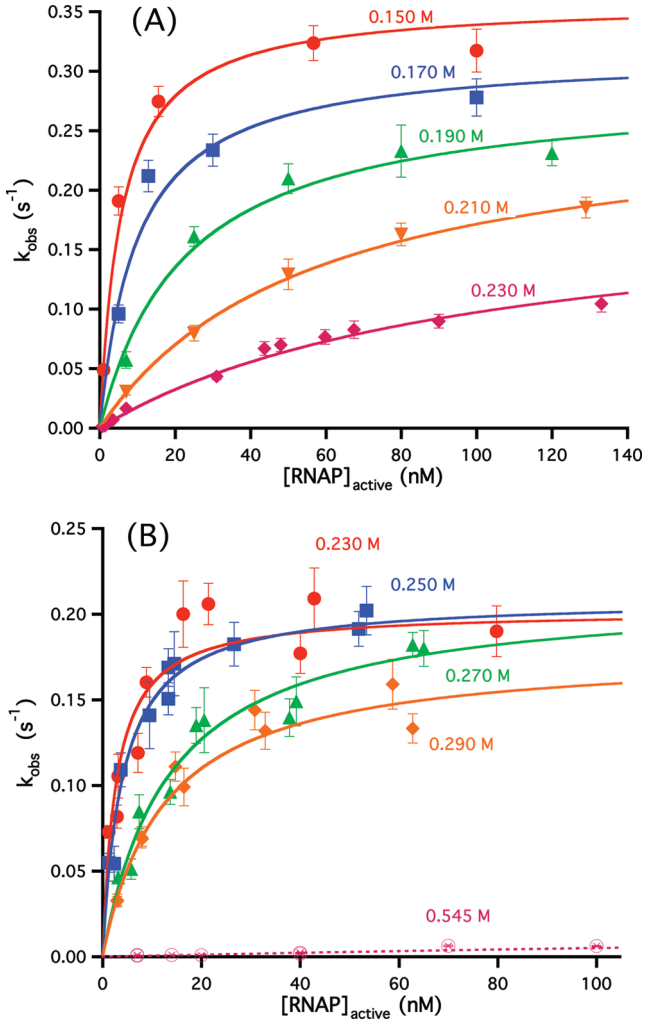

FIGURE 3: Irreversible forward rate constant k_{obs} plotted as a function of the total, active RNAP concentration at five different Na^+ concentrations in Cl^- buffer (cf. Figure 1) (A) and in Glu^- buffer (cf. Figure 2) (B). With the exception of data obtained by manual mixing at 0.55 M Na^+ in Glu^- buffer, data were obtained by rapid mixing and nonlinearly fit to eq 2, yielding values of K_1, k_2, and k_a (see Table 1) for each Na^+ concentration investigated.

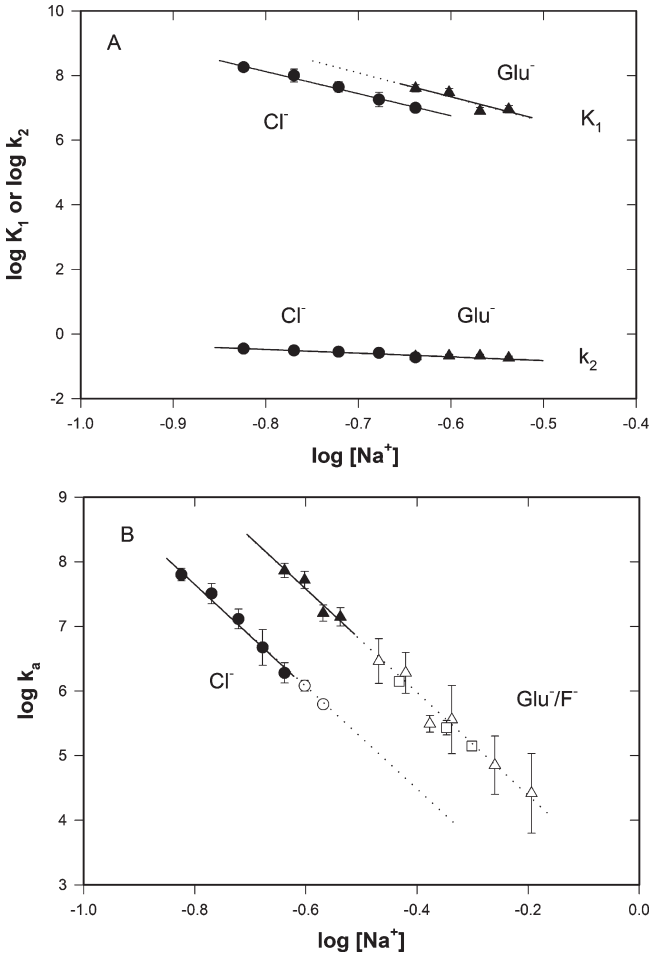

FIGURE 4: Log−log Na^+ concentration dependence of K_1, k_2, and k_a as a function of anion. (A) Data from rapid mixing experiments (cf. Figure 3) fit to eq 2 allow a dissection of k_a ($=K_1k_2$) into individual values of K_1 and k_2 in Cl^- (●) and Glu^- (▲) buffers. (B) Values of log k_a as a function of log[Na^+] in Cl^- (circles), Glu^- (triangles), and F^- (squares) buffers. Filled and empty symbols represent values of k_a obtained using rapid and manual mixing, respectively. Dashed lines represent linear extrapolations of the log−log fits to the individual data sets, drawn for comparison with individual determinations of k_a at higher salt concentrations (cf. Table 1B). Values of log−log slopes Sk_a, SK_1, and Sk_2 are given in Table 1 (see Materials and Methods for details of the fitting).

is this binding interaction? In Cl^- buffer, the binding constant K_1 for formation of I_1 decreases from 1.8×10^8 M^{-1} at 0.15 M Na^+ to 9.9×10^6 M^{-1} at 0.23 M Na^+. In Glu^- buffer at 0.23 M Na^+, K_1 is 3.6×10^8 M^{-1} and decreases to 8×10^7 M^{-1} at 0.29 M Na^+. In both Cl^- and Glu^-, logK_1 decreases linearly with log[Na^+] with slopes [$SK_1 = d(\log K_1)/d(\log[salt])$] that are the same within uncertainty ($SK_1 = -6.8 \pm 0.3$ in Cl^-, and $SK_1 = -7.5 \pm 2.3$ in Glu^-; see Figure 4A and Table 1). Fitting both data sets together yields an SK_1 value of -6.9 ± 0.3. These are large salt concentration dependences, but not nearly as large as expected from consideration of the size of the interface (see Discussion).

At 0.23 M Na^+, the only salt concentration where the data sets overlap, the value of K_1 in Glu^- buffer exceeds that in Cl^- by a factor of ~30. This is the same factor by which the log−log plots of k_a versus Na^+ concentration in Figure 4B are displaced. Such a large effect of replacing Cl^- with Glu^- on K_1 is likely a Hofmeister salt effect, based on the observation that fluoride and glutamate have very similar effects on k_a ($=K_1k_2$).

Replacement of Cl^- with Glu^- Increases the Second-Order Association Rate Constant k_a by ~30-fold at All Salt Concentrations. Above 0.23 M Na^+ in Cl^- buffer and 0.29 M Na^+ in Glu^- buffer, the equilibrium constant K_1 for I_1 formation becomes too small to allow us to dissect k_{obs} into K_1 and k_2. At higher salt concentrations, we find that k_{obs} increases linearly with RNAP concentration, as shown in Figure 3B in Glu^- buffer at 0.55 M Na^+. Linearity indicates that K_1[RNAP] ≪ 1 over the accessible range of RNAP concentrations. In this limit, the second-order association rate constant $k_a \approx k_{obs}/$[RNAP] (see eq 3), where the quality of the last approximation can be estimated by extrapolation of the log−log plots of K_1 versus [RNAP] (Figure 4A). Although individual values of K_1 and k_2 cannot be determined in this higher salt concentration range, measurements of k_{obs} at a low RNAP concentration (typically 7 nM) were performed in Cl^-, Glu^-, and F^- buffers up to the highest Na^+ concentration accessible in each to test for curvature of the log−log plots arising from Hofmeister effects (*32*). All determinations of k_a are listed in Table 1 and plotted in Figure 4B as a log−log plot together with those obtained from the data of Figure 3. A much wider range of high Na^+ concentrations can be investigated in Glu^- and F^- buffers because k_d is much smaller in

Table 1: Values of k_a, K_1, and k_2 as a Function of Na^+ and Anion (Cl^-, Glu^-, or F^-) for RP_o Formation at the λP_R Promoter at 25 °C[a]

		k_a (M^{-1} s^{-1})			K_1 (M^{-1})		k_2 (s^{-1})	
	[Na^+] (M)	Cl^-	Glu^-	F^-	Cl^-	Glu^-	Cl^-	Glu^-
A	0.15	$(6.3 \pm 0.6) \times 10^7$			$(1.8 \pm 0.2) \times 10^8$		$(3.5 \pm 0.1) \times 10^{-1}$	
	0.17	$(3.2 \pm 0.5) \times 10^7$			$(1.0 \pm 0.2) \times 10^8$		$(3.1 \pm 0.1) \times 10^{-1}$	
	0.19	$(1.3 \pm 0.2) \times 10^7$			$(4.4 \pm 0.7) \times 10^7$		$(2.8 \pm 0.2) \times 10^{-1}$	
	0.21	$(4.7 \pm 1.3) \times 10^6$			$(1.8 \pm 0.4) \times 10^7$		$(2.6 \pm 0.3) \times 10^{-1}$	
	0.23	$(1.9 \pm 0.3) \times 10^6$	$(7.3 \pm 0.8) \times 10^7$		$(9.9 \pm 1.2) \times 10^6$	$(3.6 \pm 0.4) \times 10^8$	$(1.9 \pm 0.2) \times 10^{-1}$	$(2.0 \pm 0.1) \times 10^{-1}$
	0.25		$(5.2 \pm 0.7) \times 10^7$			$(2.5 \pm 0.3) \times 10^8$		$(2.1 \pm 0.1) \times 10^{-1}$
	0.27		$(1.6 \pm 0.2) \times 10^7$			$(7.3 \pm 0.8) \times 10^7$		$(2.1 \pm 0.1) \times 10^{-1}$
	0.29		$(1.4 \pm 0.2) \times 10^7$			$(8.0 \pm 0.9) \times 10^7$		$(1.8 \pm 0.1) \times 10^{-1}$
	SK[b]	-8.0 ± 0.6	-8.0 ± 1.7		-6.8 ± 0.3	-7.5 ± 2.3	-1.1 ± 0.2	-0.9 ± 0.3
B	0.25	$(1.2 \pm 0.1) \times 10^6$						
	0.27	$(6.2 \pm 0.3) \times 10^5$						
	0.34		$(2.9 \pm 1.0) \times 10^6$					
	0.37			$(1.4 \pm 0.1) \times 10^6$				
	0.38		$(1.9 \pm 0.6) \times 10^6$					
	0.42		$(3.1 \pm 0.4) \times 10^5$					
	0.45			$(2.7 \pm 0.3) \times 10^5$				
	0.46		$(3.6 \pm 1.9) \times 10^5$					
	0.50			$(1.4 \pm 0.1) \times 10^5$				
	0.55		$(7.1 \pm 3.2) \times 10^4$					
	0.64		$(2.6 \pm 1.6) \times 10^4$					
	SK[c]	-8.0 ± 0.2	-8.3 ± 0.2					

[a]For 0.15−0.23 M Na^+ in Cl^- buffer and 0.23−0.29 M Na^+ in Glu^- buffer (section A of the table), values of k_a, K_1, and k_2 were determined from fits of rapid quench mixing data to eq 2. In section B, at higher Na^+ concentrations, values of k_a in Cl^-, Glu^- and F^- buffers were determined from fits of manual mixing data to eq 3; individual values of K_1 and k_2 cannot be determined at these salt concentrations from values of k_{obs} covering the accessible range of [RNAP] (see the text). [b]Values of $SK = -d(\log X)/d(\log[Na^+])$, where $X = k_a$, K_1, or k_2 were determined from fits of the data in section A of the table. [c]Values of *SK* were determined from fitting data from sections A and B.

Glu^- and F^- buffers than in Cl^-. Over the full range of Glu^- (or F^-) concentrations investigated, k_a decreases by more than 3 orders of magnitude (from 7.3×10^7 M^{-1} s^{-1} at 0.23 M Na^+ to 2.6×10^4 M^{-1} s^{-1} at 0.64 M Na^+). These log−log plots are linear and parallel within the uncertainty over the entire accessible salt concentration range in both Cl^- ($Sk_a = -8.0 \pm 0.2$) and Glu^-/F^- ($Sk_a = -8.3 \pm 0.2$). The offset corresponds to the ~30-fold faster association in Glu^- versus that in Cl^-. This difference is entirely the result of the difference in K_1.

Disassembly of the RNAP Clamp/Jaw in Dissociation of RP_o Complexes in Glu^- Is Remarkably Slower and Much Less Dependent on Salt Concentration Than in Cl^-. Dissociation kinetic studies probe the steps of disassembly of the clamp/jaw (conversion of RP_o to I_2) and DNA closing [conversion of I_2 to $(I_1-I_2)^\dagger$] (*24*, *27*). Irreversible dissociation data at 25 °C in 0.23−0.29 M Na^+ in Cl^- buffer are plotted in Figure 5 as θ_t^{open} versus time and fit to a single-exponential decay equation (eq 4). To show the quality of these single-exponential fits, the inset in Figure 5 plots θ_t^{open} versus log *t*; essentially 100% of the decay is described by the fit with dissociation rate constant k_d. This indicates that the steps that convert the final open complex RP_o to the kinetically significant, open intermediate I_2 rapidly equilibrate on the time scale of the dissociation rate-determining conversion of I_2 to the closed intermediate I_1. (The presence of the competitor heparin eliminates I_1 complexes.) Values of k_d increase by one order of magnitude with this 25% increase in salt concentration (from 2.9×10^{-4} s^{-1} at 0.23 M Na^+ to 2.4×10^{-3} s^{-1} at 0.29 M Na^+); these are plotted on a log−log scale versus Na^+ concentration in Figure 6. The plot is linear with a slope Sk_d of 9.2 ± 0.1, consistent with a previous determination for this promoter in its natural context (*10*).

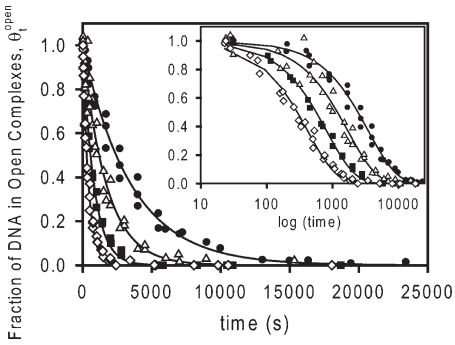

FIGURE 5: Kinetics of the irreversible dissociation of open complexes at the λP_R promoter in NaCl buffer at 25 °C. Representative values of θ_t^{open} as a function of time (*t*) determined using nitrocellulose filter binding at four different Na^+ concentrations: 0.23 (●), 0.25 (△), 0.27 (■), and 0.29 M (◇). Theoretical curves through the data are the best fits to eq 4; corresponding first-order dissociation rate constants (k_d) for each RNAP concentration are given in Table 2. Inset replots θ_t^{open} as a function of log *t*, demonstrating the single-exponential character of the kinetics over the entire time range.

By contrast, dissociation in Glu^- is extraordinarily slow at 25 °C and much less dependent on salt concentration. Attempts to directly determine k_d at 0.33 and 0.6 M Na^+ in Glu^- buffer, using a very high competitor concentration (2.5 mg/mL heparin) in an attempt to ensure irreversibility, exhibited very slow dissociation with rate constants in the range of $10^{-5}-10^{-6}$ s^{-1}, orders of magnitude slower than in Cl^- at lower salt concentrations (Figure 6). Permanganate footprinting of these 25 °C promoter complexes as a function of Na^+ concentration in Glu^- buffer shows them to be open in the vicinity of the transcription start site over the range 0.13−0.6 M Na^+ (T. J. Gries, unpublished observations).

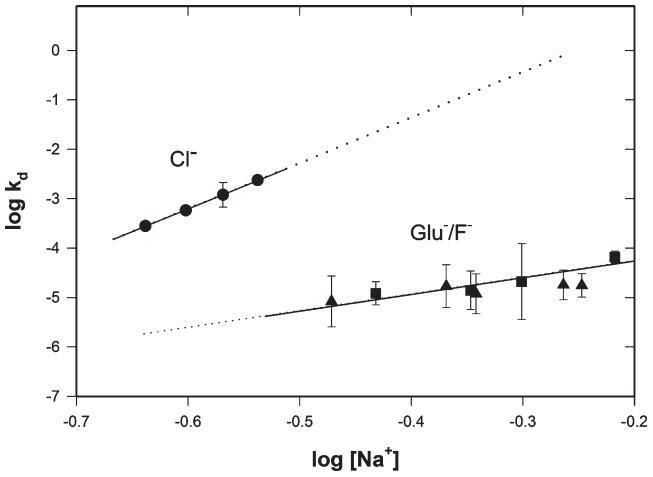

FIGURE 6: Log−log plot of dissociation rate constants (k_d) of RNAP−λP_R promoter open complexes as a function of Na^+ concentration in Cl^- and in Glu^- or F^- buffers at 25 °C. Values of k_d in Cl^- are from irreversible dissociation experiments depicted in Figure 5; values of k_d in Glu^- and F^- are from relaxation experiments like those depicted in Figure 7. Values of k_d are reported in Table 2.

Table 2: Values of k_d as a Function of Na^+ and Anion (Cl^-, Glu^-, or F^-) for the Dissociation of RP_o at the λP_R Promoter at 25 °C[a]

	k_d (s^{-1})		
[Na^+] (M)	Cl^-	Glu^-	F^-
0.23	$(2.8 \pm 0.1) \times 10^{-4}$		
0.25	$(5.8 \pm 0.4) \times 10^{-4}$		
0.27	$(1.2 \pm 0.3) \times 10^{-3}$		
0.29	$(2.37 \pm 0.09) \times 10^{-3}$		
0.34		$(8 \pm 4) \times 10^{-6}$	
0.37			$(1.2 \pm 0.3) \times 10^{-5}$
0.43		$(1.7 \pm 0.7) \times 10^{-6}$	
0.45			$(1.4 \pm 0.5) \times 10^{-5}$
0.46		$(1.2 \pm 0.5) \times 10^{-5}$	
0.50			$(2.1 \pm 0.2) \times 10^{-5}$
0.55		$(1.8 \pm 0.5) \times 10^{-5}$	
0.57		$(1.8 \pm 0.4) \times 10^{-5}$	
0.61			$(6.5 \pm 0.8) \times 10^{-5}$
Sk_d	9.2 ± 0.1	3.2 ± 0.8	

[a]Values of k_d in Glu^- and F^- buffer determined using a decay-to-equilibrim experiment [eqs 5 and 6 (see Data Analysis)] at 25 °C. $Sk_d \equiv \partial(\log k_d)/\partial(\log[Na^+])$. Values of k_d in Glu^- do not differ from those in F^- outside of experimental uncertainty and were fit together to determine Sk_d.

As an alternative, faster, and more robust method for determining k_d at 25 °C as a function of Na^+ concentration in Glu^- buffer, we observed the kinetics of approach to promoter binding equilibrium in experiments performed at very low, constant RNAP concentrations, maintained by using heparin as an RNAP buffer. In these experiments, RNAP was initially equilibrated with excess heparin and subsequently mixed with promoter DNA to initiate formation of the open complex, which is reversible in excess heparin because the free RNAP concentration is so low.

Representative results at 0.46 M Na^+ in Glu^- buffer are shown in Figure 7 as plots of θ_t^{open} as a function of time for different heparin concentrations. In these experiments, $[heparin]_{total} \gg [RNAP]_{total} \gg [promoter]_{total}$. The free RNAP concentration is very small [generally $[RNAP]_{free} < [promoter\ DNA]_{total}$ (see Table 3 of the Supporting Information)] because almost all RNAP is bound to heparin under the conditions of these experiments. Though not in excess, the free RNAP concentration

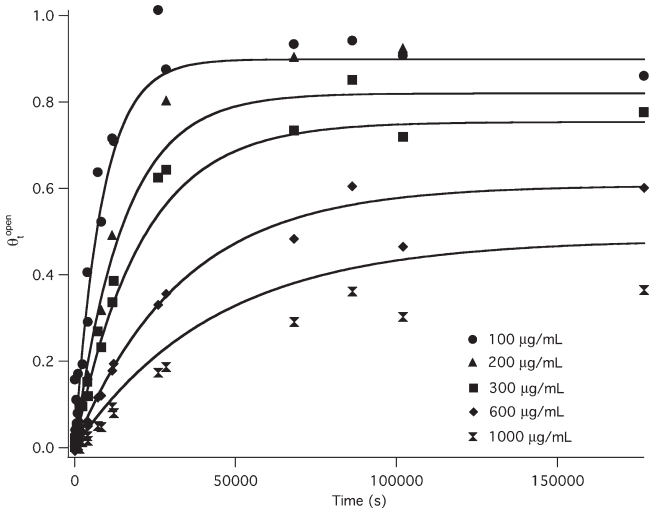

FIGURE 7: Decay-to-equilibrium kinetics of promoter association and dissociation at high glutamate (25 °C, 0.46 M Glu^-) and low, constant RNAP concentrations buffered by heparin. The fraction of promoter DNA in open complexes θ_t^{open} is plotted as a function of t, where t is the time after addition of promoter DNA (final concentration of 12.5 pM) to a solution of RNAP (total concentration of 10 nM) and heparin at total concentrations of 100, 200, 300, 600, and 1000 μg/mL. Data points from two independent experiments at each heparin concentration are plotted, except for that at 200 μg/mL which was done once. Fits shown are to the single-exponential decay-to-equilibrium kinetic equations derived for this situation (eqs 5 and 6 in Data Analysis). From the relaxation rate constant k_r, analyzed using the best fit value of the association rate constant k_a for these conditions (Figure 4B), the dissociation rate constant k_d, the free RNA polymerase concentration, and the equilibrium binding constant $K_{heparin}$ for binding RNAP to heparin are determined (see Table 2 and Table 3 of the Supporting Information).

is constant throughout the time course of reversible association because it is buffered by the heparin binding equilibrium. The heparin binding equilibrium is found to be established rapidly on the time scale of the promoter binding equilibrium, which takes many hours, so the observed kinetics are entirely the approach to equilibrium of promoter binding. The first-order rate constants obtained from single-exponential fits to these data (see Materials and Methods) are relaxation rate constants k_r, which are the sum of the pseudo-first-order (constant RNAP concentration) association rate constant ($k_a[R]_{free}$) and the dissociation rate constant k_d (see Table 3 of the Supporting Information). Hence, these decay-to-equilibrium experiments are less time-consuming than direct dissociation experiments. To obtain an accurate value for k_d from k_r, independently determined values of k_a at each of these Na^+ concentrations in Glu^- and F^- buffers (Table 1) were used. Consequently, k_d is well-determined, especially for conditions where $k_d \geq k_a[R]_{free}$.

Values of k_d obtained from the analyses of the data depicted in Figure 7 and comparable series of reversible polymerase−promoter binding experiments performed over a range of Na^+ concentrations in Glu^- and F^- buffers are listed in Table 2 and plotted in Figure 6 as a log−log plot versus Na^+ concentration to compare with the behavior of k_d in Cl^- buffer. Values of k_d in Glu^- and F^- buffers fall on a common line on this log−log plot, greatly offset from k_d values in Cl^- buffer, and with a much shallower slope ($Sk_d = 3.2 \pm 0.8$ for Glu^-/F^- vs $Sk_d = 9.2 \pm 0.1$ for Cl^-).

At 0.31 M Na^+, the salt concentration requiring the least extrapolation of the data sets in Figure 6, k_d is $\sim 10^3$-fold larger in Cl^- than in Glu^- or F^- buffer. This ratio is predicted to increase with increasing salt concentration if the log−log plot remains

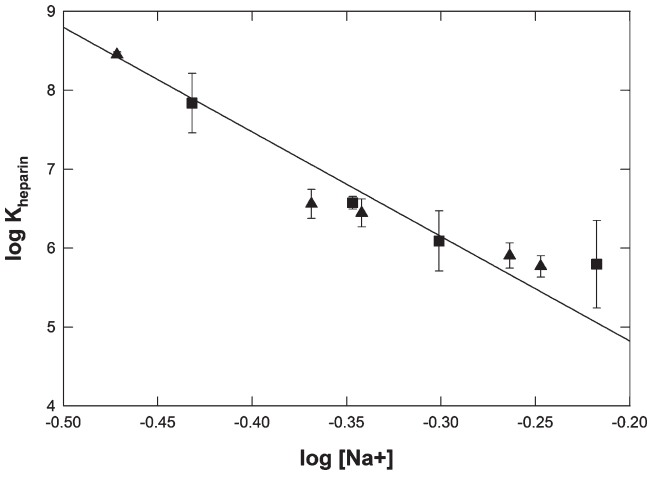

FIGURE 8: Log−log plot of the heparin binding constant $K_{heparin}$ as a function of Na^+ concentration for experiments in Glu^- and F^- buffers at 25 °C. A linear fit of these data yields $SK_{heparin}$ = d(log $K_{heparin}$)/d(log[Na^+]) = −13.2 ± 0.8 and an extrapolated 1 M Na^+ intercept of 2.2 ± 0.3.

linear in Cl^- buffer. These differences in magnitude and log−log salt derivative of k_d between Cl^- and F^- or Glu^- are very large, exceeding those previously observed for equilibrium and rate constants of other protein processes, and also contrast with the behaviors seen in Figure 4 for K_1, k_2, and k_a (see Discussion), indicating that very different conformational changes and interfaces are involved in these different steps.

For all determinations of k_d from k_r, the constant free RNAP concentration at each heparin concentration investigated is also obtained. Values of the free RNAP concentration range from $\sim 10^{-12}$ M at low Na^+ concentrations and high heparin concentrations to $\sim 10^{-10}$ M at high Na^+ and low heparin concentrations. Analysis of these decay-to-equilibrium experiments as a function of heparin concentration at a constant salt concentration provides no evidence for subunit dissociation of the RNAP holoenzyme under any condition investigated. From these free RNAP concentrations, values of the heparin binding constant $K_{heparin}$ were obtained at each Na^+ concentration investigated in Glu^- and F^- buffers. Values of $K_{heparin}$ are plotted as a log−log plot versus Na^+ concentration in Figure 8. In Glu^- and F^- buffers, the salt concentration dependence of $K_{heparin}$ ($SK_{heparin}$ = −13 ± 0.2) is similar to that of the RNAP−promoter binding constant [$SK_{obs} = Sk_a - Sk_d = -(8.3 \pm 0.2) - (3.2 \pm 0.8) = -(11.5 \pm 1.0)$].

DISCUSSION

Here we propose interpretations of the effects of salt concentration and the difference between effects of Glu^- and F^- versus Cl^- on the steps of formation of the open complex in terms of extant structural and thermodynamic characterizations of each step. Qualitative comparisons are also made with the effects of these salts on other protein−DNA interactions, on protein folding and DNA melting, and on model processes. Both the similarity of the effects of Glu^- and F^- and the large differences between effects of these anions and of Cl^- on the early and late steps of open complex formation indicate that these are Hofmeister effects and that they arise from greater exclusion of Glu^- and F^- than of Cl^- from nonpolar hydrocarbon surface, as proposed for protein folding (*17*) and for IHF−H′DNA binding (*32*). Figure 9 presents an overview of the steps, proposed conformational changes, and the effects of salt concentration and anion on each. We discuss how the Glu^- results here are predicted to affect σ^{70} holoenzyme interactions at strong promoters in vivo during the adaptation to an osmotic upshift.

Opening of the Initiation Bubble (−11 to +2) in the Active Site Cleft Is Surprisingly Insensitive to Salt Concentration and Anion: Implications for Regulation of RP_o Formation. In many biochemical processes, including enzyme catalysis and active transport, rapidly reversible initial and final steps bracket a bottleneck step that performs the key biological function (e.g., catalysis/transport). In these cases, regulation is largely achieved by effects of ligands or solutes on the rapidly reversible initial and final steps, but not on the key central catalytic/transport step of the mechanism. In RP_o formation, the first and last steps rapidly equilibrate on the time scale of the cooperative DNA opening step (*23*). Here and in our previous work, we find large effects of salt concentration, anion, and solute on the initial and final steps, but not on the central bottleneck step that converts closed complex I_1 to unstable open complex I_2. An exception is the action of far upstream DNA as an effector ligand. Truncation of DNA upstream of position −47 greatly reduces the opening rate because it reduces the extent of insertion of downstream duplex DNA in the active site cleft in I_1, thereby changing the nature of this intermediate (*33*).

Such a regulatory strategy would appear to be well-suited to organisms like *E. coli* that grow over a wide range of solution conditions, or in general to any cell responding to changes in environment. Clearly, to reprogram genetic expression, DNA opening is required regardless of solution conditions in the cell. The response to changes in growth conditions utilizes differences in promoter sequence, and/or shifts in the concentrations of σ factors, "feedback" solutes (KGlu), and stress factors (ppGpp). It will be important to determine whether these factors act to increase or decrease levels of I_1 or I_2, leaving the opening step unaffected, or whether they affect structural features of I_1 or I_2 that are central for DNA opening.

The small magnitudes of the salt concentration dependences of both rate constants of the DNA opening step (Sk_2 = −1, Sk_{-2} = 0, and SK_2 = −1) contrast with the situation for DNA melting in solution, which is significantly more dependent on salt concentration (*24*). Indeed, this weak salt concentration dependence of DNA opening by RNAP appears to be inconsistent with proposed mechanisms based on structural data in which DNA opening occurs outside (above) the active site channel (*34*−*36*). To explain the small salt dependence of opening in the active site cleft, we propose that these very small effects of salt concentration on a process (DNA opening) that is strongly dependent on salt concentration in solution may indicate that the backbones of both DNA strands interact with polymerase throughout the process, and/or that compensation is present between ion uptake and release. Possibly loading DNA as a duplex in the highly positively charged cleft in I_1 (see below) neutralizes the charge in the region (−11 to +2) opened in forming I_2. The subsequent movement of the template strand into the active site might then involve an exchange of basic contacts at the top of the cleft for those at the bottom, thereby buffering it from changes in salt concentration. Compensations in the exchange between the anionic N-terminal domain of σ^{70} (region 1.1) and the single strands in the channel (as well as unwrapping upstream DNA) may lead to small net changes in ASA, which in turn result in a small net change in binding free energy for the formation of I_2 from I_1. In addition, opening occurs in a deep cleft

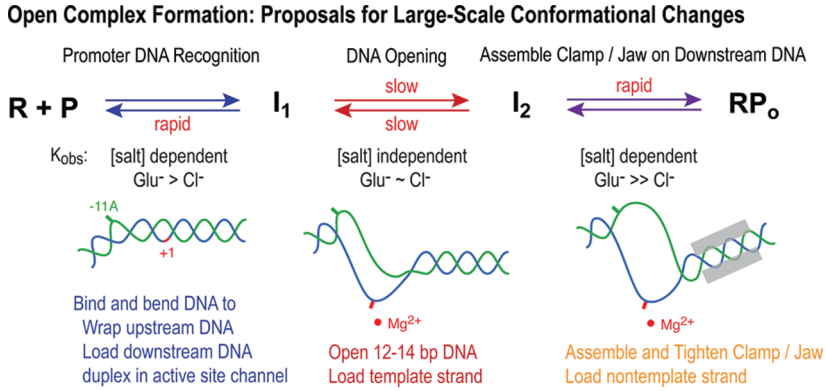

FIGURE 9: Overview of the steps of RP_o formation, proposed conformational changes, and effects of salt concentration and anion on each. Schematic based on results reported here and in refs *21*, *22*, *23*, *26*, *33*.

that is bounded by highly conserved structural features on the large subunits (*37*), which may in some way isolate the process from the bulk solution.

For the λP_R promoter at typical salt concentrations, the initial open complex I_2 is unstable relative to I_1 at low temperatures (< 15 °C), highly unstable relative to RP_o at higher temperatures (*23*), and therefore only transiently populated at any temperature. Binding free energy [specifically a favorable entropy change, since the net enthalpy change for conversion of I_1 to I_2 is +25 (*20*, *23*)] drives the opening of the DNA in the channel. However, the small magnitude of SK_2 indicates that ion release is not the origin of the favorable entropy change for this step.

While the thermodynamic origins of this driving force remain unclear, we propose the following series of structural events drive opening in the conversion of I_1 to I_2. Repositioning of σ region 1.1 in response to loading duplex DNA in the cleft in I_1 allows the strands to descend further into the channel in $(I_1-I_2)^{\ddagger}$, increasing the bending distortion at positions −12 and −11. This change likely exposes bases in the −10 hexamer on the nontemplate strand (*38*) which are "captured" by the conserved aromatic side chains on region 2 of σ (*39*−*42*). Additionally, a gradient of positive charge may exist in the channel, increasing from the top to the bottom. Such a distribution of lysines and arginines could help bring the template strand down to the base of the cleft once region 1.1 has moved.

For the entire bubble to open, we propose that a highly conserved region on the downstream lobe of β known as fork loop 2 [*Thermus thermophilus* (*T. th.*) 413−430, *E. coli* 533−550 (*37*)] may insert in the minor groove of the DNA duplex, as the DNA descends, prying apart the strands and helping to stabilize the open bubble surrounding +1. By analogy with base flipping enzymes, this insertion would further unwind the helix and create an additional ~90° bend near positions −2 and −1. In the crystal structure of the *T. th.* transcription elongation complex, fork loop 2 is positioned between the nontemplate strand and the backbone of the RNA product (*43*).

Conversion of the Unstable Open Complex I_2 to the Stable Open Complex RP_o: Evidence for Large-Scale Folding and Assembly of a Clamp/Jaw on Downstream DNA. The finding here that replacement of Cl^- with Glu^- (or F^-) greatly increases the lifetime of RP_o at 25 °C, especially at higher Na^+ concentrations, is most consistent with a large-scale burial of hydrocarbon surface in the late steps [from which F^- and Glu^- are more completely excluded than Cl^- (*17*)]. This work and our previous studies of k_d as a function of temperature, KCl, urea, and glycine betaine all indicate that large-scale rearrangements occur in the late steps of forming RP_o (*23*, *26*). These steps exhibit a large negative heat capacity change (−1 kcal/K), comparable to that for folding a 75−100-residue globular protein; the effect of urea is consistent with folding at least 100 residues, while the effects of salt concentration and GB are consistent with formation of a significant new RNAP−DNA interface involving 10−15 DNA phosphates. The most plausible scenario is that > 100 residues in RNAP fold and bind to the downstream DNA backbone in the conversion of I_2 to RP_o (*23*, *26*).

From an analysis that predicts natively disordered regions in *E. coli* RNAP, we deduced that the regions that fold are parts of the downstream clamp and jaw of β' (*26*). Highly conserved in bacterial RNAP (*37*), the following are positioned near the downstream DNA (+5 to +20) in the FRET model of RP_o (*44*) and the TEC structure (*43*): (i) a highly positively charged helix−hairpin−helix region (*T. th.* 470−507, *E. coli* 194−232), (ii) a C-terminal region (*T. th.* 1378−1424, *E. coli* 1263−1310) adjacent to (i) and switch 5 (*37*), and (iii) the mobile downstream jaw (*T. th.* 1270−1329, *E. coli* 1142−1214). Regions (i) and (ii) form part of the "clamp" of RNAP. Strong biochemical evidence exists for interactions between the clamp and jaw and downstream DNA in RP_o. Internal deletions in the jaw (*45*) as well as binding of the negatively charged phage protein Gp2 (*46*) to the jaw strongly destabilize RP_o at various promoters, including λP_R. The helix−hairpin−helix region binds near the major groove at +10 in the TEC; deletion of *E. coli* 210−215 also strongly destabilizes RP_o (*47*). Lineage-specific sequence insertion 3 (SI3) in *E. coli* β' (*48*) likely also plays a part in the assembly of the stabilizing clamp/jaw. Comprised of a repeated sandwich−barrel−hybrid motif, β'SI3 connects to the "trigger loop" by a flexible 13-amino acid linker (*49*). Deletion of β'SI3 increases k_d at λP_R by ~4-fold (*26*). In a model of the TEC, β'SI3 is positioned near the jaw, the downstream lobe of β, and the downstream DNA from +13 to +18 (*49*).

We proposed that the clamp and jaw domains are mobile and partially disordered in I_2 and assemble on the downstream DNA in the conversion of I_2 to RP_o (*26*). Because the regions in the clamp/jaw contain runs of positive residues, their interactions with duplex DNA are predicted to release cations. Importantly, our data indicate that the RNAP machinery clamps onto the downstream DNA during the $I_2 \rightarrow RP_o$ step, after the entire transcription bubble has been untwisted and opened in the active site channel [$I_1 \rightarrow I_2$ (*22*)].

Predicting the Salt Concentration Dependence for Formation of the 100 bp Wrapped DNA Interface in Closed

Intermediate I_1. The first steps of RP_o formation discriminate promoter from nonpromoter DNA by establishing interactions between σ regions 4 and 2 and conserved 6 bp sequences at −35 and −10, respectively (*41*). However, formation of I_1 at the λP_R promoter creates an extensive interface with DNA that extends well beyond the −10 and −35 regions: protection from hydroxyl radical ($^{\bullet}$OH) or DNase I cleavage of the DNA backbone in I_1 extends to at least +20 at λP_R (*21*, *50*) [and at the $\lambda P_{RM\ up1}$ promoter (*51*)]; upstream protection from $^{\bullet}$OH cleavage at λP_R extends to approximately −85 (*21*) [also apparently at the T7A1 promoter (*54*)]. These data, interpreted using structures of the free RNAP (*35*, *52*) and a complex with a fork junction DNA [from −7 to −41 (*34*)], are most simply consistent with a model (*21*) in which upstream DNA is wrapped around RNAP and downstream DNA is bound in the active site channel created by the opposition of the β and β' subunits.[2] What is the relationship between this model of I_1 and SK_1?

In our model of I_1, approximately 62 positive [arginine (R), lysine (K), and histidine (H)] and 25 negative [aspartate (D) and glutamate (E)] side chains lie near the DNA phosphate backbone, yielding a net charge of approximately +37. With the exception of the C-terminal domain (CTD) of α [modeled using the crystal structure of the *E. coli* subunits (*55*)], this charge count is based on the *T. th.* RNAP subunits (αNTD, β, β', ω, and σ^A). However, the charged residues involved in formation of the interface from position −55 to 20 are highly conserved in bacterial RNAP. With the exception of three (R, K, and H) and three (D and E) on β predicted to contact DNA from position −11 to +5 in the model of I_1, the remainder from the count above (R, K, H, E, and D) are present in *E. coli*. While the 1:1 correspondence for charged residues in the region upstream of position −55 is more variable between *T. th.* and *E. coli*, the overall charge distribution near the upstream wrapping track (positions −70 to −85) appears to be relatively conserved. This approximate structural estimate provides a reasonable basis for predicting the contribution from neutralization of DNA phosphate charge to the observed salt concentration dependence of I_1 formation. For binding of an oligocation ligand with a charge of +37 to DNA, the predicted low salt concentration value of SK_{obs} is approximately −32 (or more negative if release of ions from the ligand contributes to SK_{obs}).

Interpretation of the Much Smaller Than Expected Effect of Salt Concentration on I_1 Formation. While interactions with the −35 and −10 hexamers involve base-specific interactions with σ^{70} regions 4 and 2, respectively, the interface in I_1 is composed of predominantly nonspecific DNA backbone interactions with the other RNAP subunits (e.g., αCTDs, β, and β'). Our estimate of SK_1 [approximately −30 (above)] is much larger in magnitude than the observed log−log dependence of K_1 on Na^+ concentration ($SK_1 \sim -7$ in both Cl^- and Glu^- buffers). This difference suggests that some process involving extensive salt ion uptake by RNAP has evolved to largely compensate for this predicted cation release from the promoter DNA in forming I_1 from free RNAP and promoter DNA. We propose two scenarios involving cation uptake that may occur in I_1 formation: disruption of surface salt bridges on RNAP coupled to formation of the interface (*32*, *56*, *57*) and the placement of duplex DNA next to negatively charged region 1.1 in the channel.

Given the juxtaposition of negative and positive charges in the upstream half of the I_1 interface, we propose that coupled salt bridge disruption acts to reduce the binding constant K_1 and the magnitude of its log−log salt derivative $|SK_1|$ and likely explains the large negative ΔC_p of this step [−1.4 kcal M^{-1} K^{-1} (*20*)]. However, the walls and floor of the DNA active site channel of RNAP are highly basic. Given this charge distribution, it seems unlikely that salt bridge disruption could offset the salt ion release from binding >20 bp of downstream duplex in the channel. What does?

In free σ^{70} RNAP, region 1.1 lies in the active site channel (*44*). Where is it in I_1? Solute probes of changes in anionic (GB) and amide (urea) surface area do not detect any signature of release of σ region 1.1 in the formation of I_1 (*26*). Instead, our estimates of the burial of anionic and amide surface in the I_1 protein−DNA interface based on structural data are completely consistent with the magnitude of effects of glycine betaine and urea on K_1. As a result, we proposed that it was most likely that region 1.1 is not expelled during the formation of I_1, remaining bound and masking the active site (*26*). It seems likely that any cation release from loading of duplex DNA in the channel must be offset by cation uptake as a result of placing the two highly negatively charged regions next to each other.

In the model of I_1, DNA downstream of +1 lies above region 1.1 (*21*, *26*). Region 1.1 has a net charge of −19 and can be modeled as a negatively charged α-helical "plug" at the N-terminus (*58*) followed by an unstructured, negatively charged coil. We speculate that positioning downstream duplex DNA next to this negatively charged single-stranded (ss) DNA mimic may be somewhat analogous to DNA triplex formation. Theoretically, the limiting law per charge ion association is 0.76 for ss DNA and 0.88 for double-stranded (ds) DNA, increasing to 0.92 in a triplex (ts). If this model is appropriate for placing 20 bp of duplex DNA near σ region 1.1, then we predict approximately five cations are taken up.

Implications of the Effects of Glu^- on the Steps of Initiation for Adaptation to Osmotic Stress in Vivo. In vitro, Gralla observed that the level of transcription from open complexes at the strong σ^{70} promoter lacUV5 decreases greatly as the KGlu concentration is increased from 0.1 to 0.4 M (*7*). If Cl^- were the cytoplasmic anionic osmolyte, such increases in K^+ concentration would cause dissociation of RNAP and many other proteins from nucleic acids. However, in Glu^-, open complexes at the strong λP_R promoter are unexpectedly long-lived over the entire salt concentration range investigated here [$k_d < 10^{-5}$ s^{-1} at 25 °C even at 0.5 M Glu^-, corresponding to a lifetime ($1/k_d$) of open complexes exceeding one day]. These data suggest that open complexes at strong σ^{70} promoters in vivo (where negative supercoiling should also favor RP_o formation) do not dissociate after an osmotic upshift but may have difficulty escaping the promoter to transcribe.

While the level of transcription from many σ^{70} holoenzyme promoters is reduced at high Glu^- concentrations, the level of transcription of osmotically regulated promoters by the σ^S holoenzyme increases (*5*, *6*). Intriguingly, in vitro DNase I footprints of σ^S RNAP−osmY promoter complexes reveal that contacts upstream of position −30 are lost as the KGlu concentration increases, allowing escape from the promoter (*7*). Gralla and co-workers deduced from these data that high

[2]While our data do not allow us to determine the order of formation of these interactions, they have been determined by fast hydroxyl radical footprinting of early complexes at the T7A1 promoter (*53*, *54*). At T7A1, interactions are first established upstream and then proceed downstream (*53*, *54*). These early intermediates at λP_R rapidly equilibrate with one another and thus are not separated in the kinetic analysis.

concentrations of K^+ and Glu^- are able to release σ^S RNAP that are poised at lower salt ion concentrations, allowing both transcription and reinitiation (*7*, *59*, *60*). By contrast, σ^{70} RNAP appears to remain bound to an open promoter complex as the salt concentration increases in Glu^- buffer (this work), but its ability to transcribe is progressively weakened (*7*). Hence, in vivo salt ion concentrations themselves appear capable both of switching transcription from one set of genes to another and of poising RNAP to rapidly start at another set when conditions change (*7*, *60*, *61*).

Gralla and co-workers observe that the ability of an anion to increase the level of σ^S transcription at osmotic genes is correlated with its position in the Hofmeister series (*8*). Since the exclusion of the Hofmeister anion Glu^- from hydrocarbon surfaces causes it to favor processes that reduce the exposure of nonpolar surface to the solution (e.g., folding, assembly, and binding) (*16*), differences in the amounts and types of surface area changes in biological processes will in turn give rise to differential effects of Glu^-.

ACKNOWLEDGMENT

We thank Alison Huckenpahler for her contributions to the glutamate association kinetic data. We thank the editor and reviewers for their help in revising the manuscript.

SUPPORTING INFORMATION AVAILABLE

Irreversible rate constants (k_{obs}) for formation of open complexes as a function of $[RNAP]_{total}$ and $[Na^+]$ in Cl^- buffer (Table 1) and in Glu^- and F^- buffers (Table 2). Fits ($K_{heparin}$ and $[R]_{free}$) of relaxation to equilibrium data (k_r) at 25 °C to yield k_d in Glu^- and F^- buffers (Table 3). This material is available free of charge via the Internet at http://pubs.acs.org.

REFERENCES

1. Cayley, S., and Record, M. T., Jr. (2003) Roles of cytoplasmic osmolytes, water, and crowding in the response of *Escherichia coli* to osmotic stress: Biophysical basis of osmoprotection by glycine betaine. *Biochemistry 42*, 12596–12609.
2. Wood, J. M. (1999) Osmosensing by bacteria: Signals and membrane-based sensors. *Microbiol. Mol. Biol. Rev. 63*, 230–262.
3. Cayley, D. S., Guttman, H. J., and Record, M. T., Jr. (2000) Biophysical characterization of changes in amounts and activity of *Escherichia coli* cell and compartment water and turgor pressure in response to osmotic stress. *Biophys. J. 78*, 1748–1764.
4. Gralla, J. D., and Vargas, D. R. (2006) Potassium glutamate as a transcriptional inhibitor during bacterial osmoregulation. *EMBO J. 25*, 1515–1521.
5. Weber, A., and Jung, K. (2002) Profiling early osmostress-dependent gene expression in *Escherichia coli* using DNA macroarrays. *J. Bacteriol. 184*, 5502–5507.
6. Cheung, K. J., Badarinarayana, V., Selinger, D. W., Janse, D., and Church, G. M. (2003) A microarray-based antibiotic screen identifies a regulatory role for supercoiling in the osmotic stress response of *Escherichia coli*. *Genome Res. 13*, 206–215.
7. Lee, S. J., and Gralla, J. D. (2004) Osmo-regulation of bacterial transcription via poised RNA polymerase. *Mol. Cell 14*, 153–162.
8. Gralla, J. D., and Huo, Y. X. (2008) Remodeling and activation of *Escherichia coli* RNA polymerase by osmolytes. *Biochemistry 47*, 13189–13196.
9. Roe, J. H., Burgess, R. R., and Record, M. T., Jr. (1984) Kinetics and mechanism of the interaction of *Escherichia coli* RNA polymerase with the λP_R promoter. *J. Mol. Biol. 176*, 495–522.
10. Roe, J. H., and Record, M. T., Jr. (1985) Regulation of the kinetics of the interaction of *Escherichia coli* RNA polymerase with the λP_R promoter by salt concentration. *Biochemistry 24*, 4721–4726.
11. Leirmo, S., Harrison, C., Cayley, D. S., Burgess, R. R., and Record, M. T., Jr. (1987) Replacement of potassium chloride by potassium glutamate dramatically enhances protein-DNA interactions in vitro. *Biochemistry 26*, 2095–2101.
12. Barkley, M. D., Lewis, P. A., and Sullivan, G. E. (1981) Ion effects on the lac repressor-operator equilibrium. *Biochemistry 20*, 3842–3851.
13. Lohman, T. M., Chao, K., Green, J. M., Sage, S., and Runyon, G. T. (1989) Large-scale purification and characterization of the *Escherichia coli* rep gene product. *J. Biol. Chem. 264*, 10139–10147.
14. Dragan, A. I., Li, Z., Makeyeva, E. N., Milgotina, E. I., Liu, Y., Crane-Robinson, C., and Privalov, P. L. (2006) Forces driving the binding of homeodomains to DNA. *Biochemistry 45*, 141–151.
15. Maslak, M., and Martin, C. T. (1994) Effects of solution conditions on the steady-state kinetics of initiation of transcription by T7 RNA polymerase. *Biochemistry 33*, 6918–6924.
16. Pegram, L. M., and Record, M. T., Jr. (2008) Thermodynamic origin of Hofmeister ion effects. *J. Phys. Chem. B 112*, 9428–9436.
17. Pegram, L. M., Wendorff, T., Erdmann, R., Shkel, I. A., Bellissimo, D., Felitsky, D. J., and Record, M. T. (2010) Why Hofmeister effects of many salts favor protein folding but not DNA helix formation. *Proc. Natl. Acad. Sci. U.S.A.* (in press).
18. Roe, J. H., Burgess, R. R., and Record, M. T., Jr. (1985) Temperature dependence of the rate constants of the *Escherichia coli* RNA polymerase-λP_R promoter interaction. Assignment of the kinetic steps corresponding to protein conformational change and DNA opening. *J. Mol. Biol. 184*, 441–453.
19. Tsodikov, O. V., and Record, M. T., Jr. (1999) General method of analysis of kinetic equations for multistep reversible mechanisms in the single-exponential regime: Application to kinetics of open complex formation between $E\sigma^{70}$ RNA polymerase and λP_R promoter DNA. *Biophys. J. 76*, 1320–1329.
20. Saecker, R. M., Tsodikov, O. V., McQuade, K. L., Schlax, P. E., Jr., Capp, M. W., and Record, M. T., Jr. (2002) Kinetic studies and structural models of the association of *E. coli* σ^{70} RNA polymerase with the λP_R promoter: Large scale conformational changes in forming the kinetically significant intermediates. *J. Mol. Biol. 319*, 649–671.
21. Davis, C. A., Bingman, C. A., Landick, R., Record, M. T., Jr., and Saecker, R. M. (2007) Real-time footprinting of DNA in the first kinetically significant intermediate in open complex formation by *Escherichia coli* RNA polymerase. *Proc. Natl. Acad. Sci. U.S.A. 104*, 7833–7838.
22. Gries, T. J., Kontur, W. S., Capp, M. W., Saecker, R. M., and Record, M. T., Jr., (2010). One-step DNA melting in the RNA polymerase cleft opens the initiation bubble to form an unstable open complex, *Proc. Natl. Acad. Sci. U.S.A.*, in press.
23. Kontur, W. S., Saecker, R. M., Capp, M. W., and Record, M. T., Jr. (2008) Late steps in the formation of *E. coli* RNA polymerase-λP_R promoter open complexes: Characterization of conformational changes by rapid [perturbant] upshift experiments. *J. Mol. Biol. 376*, 1034–1047.
24. Bloomfield, V., Crothers, D. M., and Tinoco, I., Jr., Eds. (2000) Nucleic Acids: Structures, Properties, and Functions, University Science Books, Sausalito, CA.
25. Spolar, R. S., and Record, M. T., Jr. (1994) Coupling of local folding to site-specific binding of proteins to DNA. *Science 263*, 777–784.
26. Kontur, W. S., Saecker, R. M., Davis, C. A., Capp, M. W., and Record, M. T., Jr. (2006) Solute probes of conformational changes in open complex (RP_o) formation by *Escherichia coli* RNA polymerase at the λP_R promoter: Evidence for unmasking of the active site in the isomerization step and for large-scale coupled folding in the subsequent conversion to RP_o. *Biochemistry 45*, 2161–2177.
27. Burgess, R. R., and Jendrisak, J. J. (1975) A procedure for the rapid, large-scale purification of *Escherichia coli* DNA-dependent RNA polymerase involving Polymin P precipitation and DNA-cellulose chromatography. *Biochemistry 14*, 4634–4638.
28. Gonzalez, N., Wiggs, J., and Chamberlin, M. J. (1977) A simple procedure for resolution of *Escherichia coli* RNA polymerase holoenzyme from core polymerase. *Arch. Biochem. Biophys. 182*, 404–408.
29. Craig, M. L., Suh, W. C., and Record, M. T., Jr. (1995) HO• and DNase I probing of $E\sigma^{70}$ RNA polymerase-λP_R promoter open complexes: Mg^{2+} binding and its structural consequences at the transcription start site. *Biochemistry 34*, 15624–15632.
30. Leirmo, S. (1989) The Mechanism of Interaction of *E. coli* RNA Polymerase with Bacteriophage and Bacterial Promoters. Ph.D. Thesis, Department of Biochemistry, University of Wisconsin, Madison, WI.
31. Glaser, B. T., Bergendahl, V., Anthony, L. C., Olson, B., and Burgess, R. R. (2009) Studying the salt dependence of the binding of σ^{70} and σ^{32}

to core RNA polymerase using luminescence resonance energy transfer. *PLoS One 4*, e6490.
32. Vander Meulen, K. A., Saecker, R. M., and Record, M. T., Jr. (2008) Formation of a wrapped DNA-protein interface: Experimental characterization and analysis of the large contributions of ions and water to the thermodynamics of binding IHF to H′ DNA. *J. Mol. Biol. 377*, 9–27.
33. Davis, C. A., Capp, M. W., Record, M. T., Jr., and Saecker, R. M. (2005) The effects of upstream DNA on open complex formation by *Escherichia coli* RNA polymerase. *Proc. Natl. Acad. Sci. U.S.A. 102*, 285–290.
34. Murakami, K. S., Masuda, S., Campbell, E. A., Muzzin, O., and Darst, S. A. (2002) Structural basis of transcription initiation: An RNA polymerase holoenzyme-DNA complex. *Science 296*, 1285–1290.
35. Vassylyev, D. G., Sekine, S., Laptenko, O., Lee, J., Vassylyeva, M. N., Borukhov, S., and Yokoyama, S. (2002) Crystal structure of a bacterial RNA polymerase holoenzyme at 2.6 Å resolution. *Nature 417*, 712–719.
36. Murakami, K. S., and Darst, S. A. (2003) Bacterial RNA polymerases: The wholo story. *Curr. Opin. Struct. Biol. 13*, 31–39.
37. Lane, W. J., and Darst, S. A. (2010) Molecular evolution of multisubunit RNA polymerases: Structural analysis. *J. Mol. Biol. 395*, 686–704.
38. Schroeder, L. A., Gries, T. J., Saecker, R. M., Record, M. T., Jr., Harris, M. E., and DeHaseth, P. L. (2009) Evidence for a tyrosine-adenine stacking interaction and for a short-lived open intermediate subsequent to initial binding of *Escherichia coli* RNA polymerase to promoter DNA. *J. Mol. Biol. 385*, 339–349.
39. Tomsic, M., Tsujikawa, L., Panaghie, G., Wang, Y., Azok, J., and deHaseth, P. L. (2001) Different roles for basic and aromatic amino acids in conserved region 2 of *Escherichia coli* σ^{70} in the nucleation and maintenance of the single-stranded DNA bubble in open RNA polymerase-promoter complexes. *J. Biol. Chem. 276*, 31891–31896.
40. Schroeder, L. A., Karpen, M. E., and deHaseth, P. L. (2008) Threonine 429 of *Escherichia coli* σ^{70} is a key participant in promoter DNA melting by RNA polymerase. *J. Mol. Biol. 376*, 153–165.
41. Helmann, J. D., and deHaseth, P. L. (1999) Protein-nucleic acid interactions during open complex formation investigated by systematic alteration of the protein and DNA binding partners. *Biochemistry 38*, 5959–5967.
42. Fenton, M. S., Lee, S. J., and Gralla, J. D. (2000) *Escherichia coli* promoter opening and −10 recognition: Mutational analysis of σ^{70}. *EMBO J. 19*, 1130–1137.
43. Vassylyev, D. G., Vassylyeva, M. N., Perederina, A., Tahirov, T. H., and Artsimovitch, I. (2007) Structural basis for transcription elongation by bacterial RNA polymerase. *Nature 448*, 157–162.
44. Mekler, V., Kortkhonjia, E., Mukhopadhyay, J., Knight, J., Revyakin, A., Kapanidis, A. N., Niu, W., Ebright, Y. W., Levy, R., and Ebright, R. H. (2002) Structural organization of bacterial RNA polymerase holoenzyme and the RNA polymerase-promoter open complex. *Cell 108*, 599–614.
45. Ederth, J., Artsimovitch, I., Isaksson, L. A., and Landick, R. (2002) The downstream DNA jaw of bacterial RNA polymerase facilitates both transcriptional initiation and pausing. *J. Biol. Chem. 277*, 37456–37463.
46. Camara, B., Liu, M., Reynolds, J., Shadrin, A., Liu, B., Kwok, K., Simpson, P., Weinzierl, R., Severinov, K., Cota, E., Matthews, S., and Wigneshweraraj, S. R. (2010) T7 phage protein Gp2 inhibits the *Escherichia coli* RNA polymerase by antagonizing stable DNA strand separation near the transcription start site. *Proc. Natl. Acad. Sci. U.S.A. 107*, 2247–2252.
47. Bartlett, M. S., Gaal, T., Ross, W., and Gourse, R. L. (1998) RNA polymerase mutants that destabilize RNA polymerase-promoter complexes alter NTP-sensing by rrn P1 promoters. *J. Mol. Biol. 279*, 331–345.
48. Lane, W. J., and Darst, S. A. (2010) Molecular evolution of multisubunit RNA polymerases: Sequence analysis. *J. Mol. Biol. 395*, 671–685.
49. Chlenov, M., Masuda, S., Murakami, K. S., Nikiforov, V., Darst, S. A., and Mustaev, A. (2005) Structure and function of lineage-specific sequence insertions in the bacterial RNA polymerase β' subunit. *J. Mol. Biol. 353*, 138–154.
50. Craig, M. L., Tsodikov, O. V., McQuade, K. L., Schlax, P. E., Jr., Capp, M. W., Saecker, R. M., and Record, M. T., Jr. (1998) DNA footprints of the two kinetically significant intermediates in formation of an RNA polymerase-promoter open complex: Evidence that interactions with start site and downstream DNA induce sequential conformational changes in polymerase and DNA. *J. Mol. Biol. 283*, 741–756.
51. Li, X. Y., and McClure, W. R. (1998) Characterization of the closed complex intermediate formed during transcription initiation by *Escherichia coli* RNA polymerase. *J. Biol. Chem. 273*, 23549–23557.
52. Murakami, K. S., Masuda, S., and Darst, S. A. (2002) Structural basis of transcription initiation: RNA polymerase holoenzyme at 4 Å resolution. *Science 296*, 1280–1284.
53. Rogozina, A., Zaychikov, E., Buckle, M., Heumann, H., and Sclavi, B. (2009) DNA melting by RNA polymerase at the T7A1 promoter precedes the rate-limiting step at 37 °C and results in the accumulation of an off-pathway intermediate. *Nucleic Acids Res. 37*, 5390–5404.
54. Sclavi, B., Zaychikov, E., Rogozina, A., Walther, F., Buckle, M., and Heumann, H. (2005) Real-time characterization of intermediates in the pathway to open complex formation by *Escherichia coli* RNA polymerase at the T7A1 promoter. *Proc. Natl. Acad. Sci. U.S.A. 102*, 4706–4711.
55. Benoff, B., Yang, H., Lawson, C. L., Parkinson, G., Liu, J., Blatter, E., Ebright, Y. W., Berman, H. M., and Ebright, R. H. (2002) Structural basis of transcription activation: The CAP-αCTD-DNA complex. *Science 297*, 1562–1566.
56. Holbrook, J. A., Tsodikov, O. V., Saecker, R. M., and Record, M. T., Jr. (2001) Specific and non-specific interactions of integration host factor with DNA: Thermodynamic evidence for disruption of multiple IHF surface salt-bridges coupled to DNA binding. *J. Mol. Biol. 310*, 379–401.
57. Saecker, R. M., and Record, M. T., Jr. (2002) Protein surface salt bridges and paths for DNA wrapping. *Curr. Opin. Struct. Biol. 12*, 311–319.
58. Schwartz, E. C., Shekhtman, A., Dutta, K., Pratt, M. R., Cowburn, D., Darst, S., and Muir, T. W. (2008) A full-length group 1 bacterial σ factor adopts a compact structure incompatible with DNA binding. *Chem. Biol. 15*, 1091–1103.
59. Huo, Y. X., Rosenthal, A. Z., and Gralla, J. D. (2008) General stress response signalling: Unwrapping transcription complexes by DNA relaxation via the σ^{38} C-terminal domain. *Mol. Microbiol. 70*, 369–378.
60. Rosenthal, A. Z., Kim, Y., and Gralla, J. D. (2008) Poising of *Escherichia coli* RNA polymerase and its release from the σ^{38} C-terminal tail for osmY transcription. *J. Mol. Biol. 376*, 938–949.
61. Rosenthal, A. Z., Hu, M., and Gralla, J. D. (2006) Osmolyte-induced transcription: −35 region elements and recognition by σ^{38} (rpoS). *Mol. Microbiol. 59*, 1052–1061.